Torsion Effects in a Helix Nanowire with Easy-tangential Anisotropy

Kostyantyn V. Yershov[1,2,*], *Volodymyr P. Kravchuk*[1,†], *Denis D. Sheka*[3,‡], *Yuri Gaididei*[1,§]
[1]Bogolubov Institute for Theoretical Physics, Department of Quantum Electronics, Kyiv, Ukraine
[2]National University "Kyiv-Mohyla academy", Department of Natural Sciences, Kyiv, Ukraine
[3]Taras Shevchenko National University of Kyiv, Faculty of Radio Physics, Electronics and Computer Systems, Kyiv, Ukraine
*yershov@bitp.kiev.ua, †vkravchuk@bitp.kiev.ua, ‡sheka@univ.net.ua, §ybg@bitp.kiev.ua

I. Introduction

Due to the constant curvature and torsion, a helix-shaped magnetic nanowire is a simplest system for studying of curvature and torsion effects in magnetization dynamics. Depending on the anisotropy direction different artificial complex helimagnetic-like configurations were experimentally realized: hollow-bar-, corkscrew-, and radial-magnetized 3D micro-helix coils [1]. Rolled magnetic structures are now widely discussed in the context of possible application in flexible and stretchable magnetoelectronic devices [2], rolledup GMR sensors [3], spinwave filters [4,5], and microrobots [6]. Helix coil magnetic structures have the potential to be used in a variety of bioapplication areas, such as in medical procedures, cell biology [7].

In the current study we apply previously developed theory [8] aimed to describe magnetization statics and linear dynamics in the helix wire.

II. The Model of the Wire

We consider the model of 1D curved wire $\boldsymbol{\gamma}(s)$ embedded in 3D space $\mathbb{R}^3$ with s being the arc length. For such wire it is convenient to use Frennet-Serret basis $(\boldsymbol{e}_t, \boldsymbol{e}_n, \boldsymbol{e}_b)$ with $\boldsymbol{e}_t = \boldsymbol{\gamma}'(s)$, $\boldsymbol{e}_n = \boldsymbol{\gamma}''(s)/|\boldsymbol{\gamma}''(s)|$, and $\boldsymbol{e}_b = [\boldsymbol{e}_t, \boldsymbol{e}_n]$ being tangential, normal, and binormal unit vectors respectively. Here and below prime denotes to the derivatives with respect to s.

Using the Frennet-Serret basis one can introduce the angular magnetization parameterization

$$\boldsymbol{m} = \sin\theta\cos\varphi\, \boldsymbol{e}_t + \sin\theta\sin\varphi\, \boldsymbol{e}_n + \cos\theta\, \boldsymbol{e}_b\,, \qquad (1)$$

where $\boldsymbol{m} = \boldsymbol{M}/M_s$ is normalized magnetization unit vector with M_s being the saturation magnetization.

Magnetization dynamics can be described by the phenomenological Landau-Lifshitz equations

$$-\sin\theta\,\partial\theta/\partial t = \omega_0\,\delta E/\delta\varphi, \qquad \sin\theta\,\partial\varphi/\partial t = \omega_0\,\delta E/\delta\theta, \qquad (2)$$

where frequency $\omega_0 = 4\pi\gamma_0 Ms$ determines the characteristic time scale with γ_0 being the gyromagnetic ratio, E is a total energy normalized by the $4\pi Ms^2$.

We start with the a simple model, which take into account only two contributions to the total magnetic energy:

$$E = S\int[l^2\,\varepsilon_{ex} - k_t\sin^2\theta\cos^2\varphi]ds, \qquad (3)$$

here S is cross-section area, $l=\sqrt{(A/4\pi Ms^2)}$ is exchange length with A being exchange constant, ε_{ex} is the exchange energy density, and $k_t=K/4\pi Ms^2$ is the dimensionless anisotropy constant. Competition of the exchange and the anisotropy contributions results in the magnetic length $w= lk_t^{-1/2}$, which determines the length scale of the system. Considering the wires, with small transversal size $h<w$, we assume the magnetization spatial one-dimensionality: $\boldsymbol{m} = \boldsymbol{m}(s,t)$.

For the infinitesimally thin wires, the magnetostatic energy is completely reduced to the easy-tangential anisotropy with $k_t^d=1/4$, including case of curvilinear wire [8]. Therefore the magnetostatic interaction can be taken into account by a simple redefinition of the anisotropy constants, leading to a new magnetic length

$$k_t \to k_t^{\text{eff}} = k_t + k_d,$$
$$w \to w^{\text{eff}} = l(k_t^{\text{eff}})^{-1/2} = l(k_t + k_d)^{-1.2}. \qquad (4)$$

Thus the model (3) is physically sound also for the thin wires made of magnetically soft materials.

In terms of the angular parameterization (1) the exchange energy densities of curved wire has form [9]

$$\varepsilon_{ex} = (\theta' - \tau\sin\varphi)^2 + ((\varphi' + \kappa)\sin\theta - \tau\cos\theta\cos\varphi)^2, \qquad (5)$$

where κ is a curvature of the wire and τ is a torsion of the wire.

III. Equilibrium States of the Helix Wire

We parameterize the helix geometry using curvature and torsion in the following way

$$\boldsymbol{\gamma}(s) = (\kappa s_0^2\cos(s/s_0),\ \kappa s_0^2\sin(s/s_0),\ s_0 s\tau)$$
$$s_0 = (\kappa^2+\tau^2)^{-1/2}. \qquad (6)$$

There is one-to-one correspondence between the helix radius $R = \kappa s_0^2$, pitch $P = 2\pi\tau s_0^2$, and the curvature and torsion parameters.

To obtain the equilibrium states we must analyze the static case of Eq. (2)

$$\delta E/\delta\theta = w^2\,(\tau\cos\varphi\,(\kappa\cos 2\theta - 2\varphi'\sin^2\theta) + \theta'' - \sin\theta\cos\theta((\kappa+\varphi')^2 - \tau^2\cos^2\varphi)) - \sin\theta\cos\theta\cos^2\varphi = 0,$$

$$\delta E/\delta\varphi = w^2\,(\sin\theta\cos\theta\,(2\,\theta'\,(\kappa+\varphi') - \kappa\tau\sin\varphi) + \sin^2\theta(\varphi'' + 2\tau\cos\varphi - \tau^2\sin\varphi\cos\varphi)) + \sin^2\theta\sin\varphi\cos\varphi = 0. \qquad (7)$$

A. Quasi-tangential state

We first look for the homogeneous (in the curvilinear reference frame) solution. Such kind of solutions is possible due to the constant curvature κ and the torsion τ. We can

easily solve the static equations, see Eq. (7), using the substitution $\theta(s) = \theta^t$ and $\varphi(s) = \varphi^t$:

$$\tan\theta^t = -2C\sigma\varkappa/(1 - \varkappa^2 + \sigma^2), \qquad \varphi^t = 0, \pi, \tag{8}$$

where $C = \cos\varphi^t = \pm 1$, $\varkappa = w\kappa$ and $\sigma = w\tau$ are reduced curvature and torsion, respectively. Explicitly for magnetization angles we get

$$\theta^t = \pi/2 - \arctan(2C\sigma\varkappa/V_0), \qquad \varphi^t = 0, \pi,$$
$$V_0 = 1 - \varkappa^2 + \sigma^2 + V_1,$$
$$V_1 = ((1 - \varkappa^2 + \sigma^2)^2 + 4\varkappa^2\sigma^2)^{1/2}. \tag{9}$$

The dependence $\theta^t(\varkappa,\sigma)$ is presented in Fig. 1.

In the limit case of very small curvature and torsion ($\varkappa,\sigma \ll 1$), the magnetization distribution becomes almost tangential, see Fig. 3(a) with the asymptotic behavior

$$\theta^t = \pi/2 - C\sigma\varkappa, \text{ for } \varkappa,\sigma \ll 1. \tag{10}$$

That is why we refer to the state (9) as to the quasi-tangential state.

The energy density of Eq. (3) for the quasi-tangential state (9) reads

$$\varepsilon^t = -(1 - \varkappa^2 - \sigma^2 + V_1)/(2w^2). \tag{11}$$

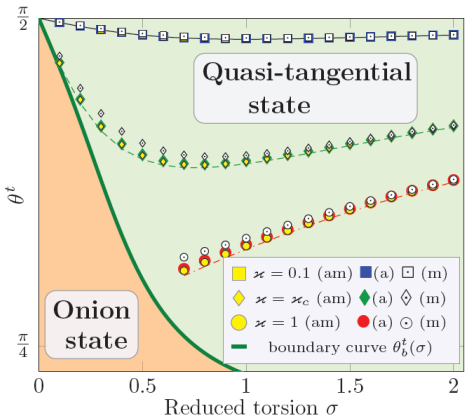

Fig. 1. Equilibrium magnetization distribution in the quasi-tangential state of the helix wire with $C = +1$. Lines correspond to the analytics, see Eq. (9). Symbols correspond to simulations with: (a) anisotropic Heisenberg magnets (k_t=1, $w = l$), (am) wires with account of dipolar interaction (k_t=1, $w^{\text{eff}} = 2l\sqrt{5}$), and (ms) isotropic wires with account of dipolar interaction (k_t= 0, $w^{\text{eff}} = 2l$).

B. Onion state

Let us discuss the case of a large curvature and torsion. We are looking for a solution periodic with respect to parameter χ. We look for solutions in the following form

$$\theta^{\text{on}} = \pi/2 - \vartheta(\chi), \quad \varphi^{\text{on}} = -\chi + \phi(\chi) \tag{12}$$

with $\vartheta(\chi)$ and $\varphi(\chi)$ being 2π periodic functions.

The symmetry of Eqs. (7) dictates the symmetry of 2π periodic functions ϑ and ϕ, which has the following Fourier expansion

$$\vartheta(\chi) = \sum\vartheta_n\cos(2n-1)\chi, \quad \phi(\chi) = \sum\phi_n\sin 2n\chi, \tag{13}$$

where we summarize over $n = 1 \ldots N$, and $N \to \infty$. By substituting Eq. (13) into the (7), one get the set of nonlinear equations for amplitudes ϑ_n and ϕ_n.

The energy of the onion state can be calculated numerically using amplitudes ϑ_n and ϕ_n as

$$\varepsilon^{\text{on}} = (2\pi)^{-1/2}\int\varepsilon(\vartheta_1 \ldots \vartheta_n; \phi_1 \ldots \phi_n)d\chi. \tag{14}$$

C. Phase diagram

By comparing energies of different states, we compute the energetically preferable states for different curvature and torsion values. The resulting phase diagram is presented in Fig. 2. There are two phases: (i) The quasi-tangential state is realized for relatively small curvatures, when $\varkappa < \varkappa_b$; in such a state the magnetization direction is close to the direction of easy-tangential anisotropy $\boldsymbol{e}_1$. (ii) The onion state corresponds to the case, when $\varkappa > \varkappa_b$; the magnetization distribution is inhomogeneous in accordance to (12) and (13).

The boundary between two phases $\varkappa_b = \varkappa_b(\sigma)$ can be derived using the condition

$$\varepsilon^t(\varkappa_b, \sigma) = \varepsilon^{\text{on}}(\varkappa_b, \sigma). \tag{15}$$

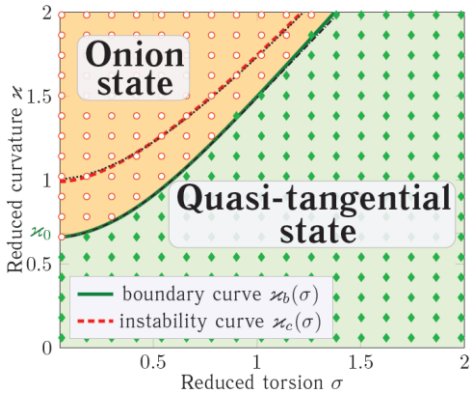

Fig. 2. Phase diagram of equilibrium magnetization states for helix wire with easy-tangential anisotropy. Symbols correspond to simulation data: green diamonds to quasi-tangential states and open circles to the onion ones.

IV. Spin Wave Spectrum of the Helix Wire

To obtain spin wave spectrum we linearized the Eq. (2) on the background of the quasi-tangential equilibrium state (9),

$$\theta(s,t) = \theta^t + \vartheta(s,t), \qquad \varphi(s,t) = \varphi^t + \phi(s,t)/\sin\theta^t. \tag{16}$$

Then for ϑ and ϕ we get the set of linear equations:

$$\partial_{t'}\phi = -\partial_{\xi\xi}\vartheta + V_1\vartheta - 2A\partial_\xi\phi, \; -\partial_{t'}\vartheta = -\partial_{\xi\xi}\phi + V_1\phi + 2A\partial_\xi\vartheta,$$
$$V_2 = (1 + \varkappa^2 + \sigma^2 + V_1)/2, \; A = 2\sigma V_2(2/(V_0V_1))^{1/2}, \tag{17}$$

where $\partial_{t'}$ is the derivative with respect to dimensionless time $t' = t\omega_0$ and ∂_ξ is the derivative with respect to dimensionless coordinate $\xi = s/w$. V_1 and V_2 appears as scalar potentials, and A acts as a vector potential $\boldsymbol{A} = \boldsymbol{e}_1 A$ of effective magnetic field. The equations on functions ϑ and ϕ can be combined in one equation for complex function $\psi = \vartheta + i\phi$,

$$-i\partial_{t'}\psi = H\psi + W\psi^*, \qquad H = (-i\partial_\xi - A)^2 + U. \tag{18}$$

This differential equation has a form of generalized Shrödinger equation, originally proposed for the description of

spin waves on the magnetic vortex background [10]. The "potentials" in (18) reads

$$U = (V_1 + V_2)/2 - A^2, \qquad W = -(1 + w^2\varepsilon^t)/2. \tag{19}$$

Now we apply the traveling wave Ansatz for the spinwave complex magnon amplitude

$$\psi(\xi,t') = ue^{i\Phi} + ve^{-i\Phi}, \qquad \Phi = q\xi - \Omega t' + \eta, \tag{20}$$

with $q=kw$ is dimensionless wave number, $\Omega=\omega/\omega_0$ the dimensionless frequency, η being arbitrary phase, and u, v being constants. By substituting the Ansatz (20) into the generalized Shrödinger equation, one can derive the spectrum of the spin waves:

$$\Omega(q) = 2Aq + ((q^2 + V_1)(q^2 + V_2))^{1/2}. \tag{21}$$

Similar to the straight wire case with $\Omega_s(q) = 1+q^2$, the spectrum of spin waves in the helix wire has a gap, caused, first of all, by the anisotropy. However its value essentially depends on the curvature and the torsion. Moreover, the spectrum gap occurs at finite $q = q_0$, see Fig. 3. This means the asymmetry in the spectrum with respect to the change $q \to -q$: spin waves have different velocities depending on the direction (along the helix axis or in opposite direction). This asymmetry in the dispersion law (21) occurs in the first term $2Aq$, which is originated from the effective Dzyaloshinskii interaction.

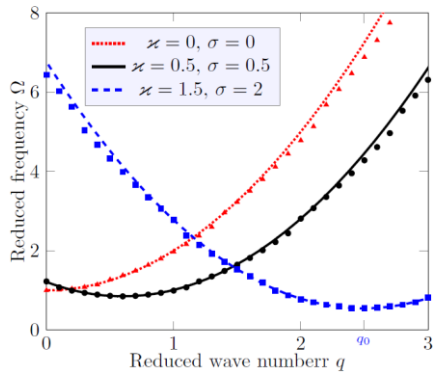

Fig. 3. Dispersion law of spinwave spectrum of the helix wire with easy-tangential anisotropy. Symbols correspond to simulation data and lines correspond to formula (21).

V. Simulations

In order to verify our analytical results we numerically simulate the magnetization dynamics of a helix-shaped chain of discrete magnetic moments. Details of the numerical procedure can be found in Ref. 11.

A. The model check

To check the model that we use in our theory we performed three different types of simulations to found the deviation of magnetic angle θ from θ^t, see Fig. 1 and Eq. (9). (i) Firstly we simulate the Heisenberg magnet with $k_t=1$ and $w=l$ (correspond to symbols (a) in Fig. 1). (ii) Then we simulate the wire with account of anisotropy and dipolar interaction with $k_t \to k_t^{\text{eff}}=5/4$ and $w \to w^{\text{eff}}=2l/\sqrt{5}$ (correspond to the case (am) in Fig. 1). (iii) Finally we simulate the soft magnet with the soft magnet with $k_t \to k_t^{\text{eff}}=1/4$ and $w \to w^{\text{eff}}=2l$ (correspond to the case (m) in Fig. 1). The results of simulation presented in Fig. 1.

B. The phase diagram of equilibrium magnetization states

To obtain equilibrium states we simulate Landau-Lifshitz equation for five different initial states, namely the tangential, onion, normal, binormal, and the random states. The final static state with the lowest energy is considered to be the equilibrium magnetization state. We obtain that for easy-tangential anisotropy exist two equilibrium states onion one and anisotropy-aligned state (quasi-tangential). We present simulations data in Fig. 2 (symbols) together with theoretical results (plotted by lines). One can see a very good agreement between simulations and analytics.

C. Dispersion relations

The magnon spectrum computation was done in two steps. Firstly the helix wire was relaxed for different wave numbers in spatially nonuniform week magnetic field with cosine form $\boldsymbol{b}^i=b_0\cos(ks^i)$, where k is a wave number, s^i numerates spin position, and b_0 field amplitude. After relaxation we switch off the magnetic field and observe the free dynamics of the system. Then space-time Fourier transformation of normal magnetization component was performed. The frequency Ω which correspond to the maximum of Fourier spectrum is marked by a symbol for a given wave number in Fig. 3.

VI. Conclusion

In conclusion, we have presented a detailed study of statics and linear dynamics of magnetization in the helix wire with easy-tangential anisotropy. We have described equilibrium magnetization states and present them in form of the phase diagram, see Fig. 2. Also we have shown that the magnon spectrum of the helix wire experiences an asymmetry caused by the torsion.

References

[1] E. J. Smith, D. Makarov, S. Sanchez, V. M. Fomin, and O. G. Schmidt, Phys. Rev. Lett. 107, 097204 (2011).

[2] R. Streubel, J. Lee, D. Makarov, M.-Y. Im, D. Karnaushenko, L. Han, R. Schafer, P. Fischer, S.-K. Kim, and O. G. Schmidt, Advanced Materials 26, 316 (2014).

[3] I. Monch, D. Makarov, R. Koseva, L. Baraban, D. Karnaushenko, C. Kaiser, K.-F. Arndt, and O. G. Schmidt, ACS Nano 5, 7436 (2011).

[4] F. Balhorn, S. Mansfeld, A. Krohn, J. Topp, W. Hansen, D. Heitmann, and S. Mendach, Physical Review Letters 104, 037205 (2010).

[5] F. Balhorn, C. Bausch, S. Jeni, W. Hansen, D. Heitmann, and S. Mendach, Phys. Rev. B 88, 054402 (2013).

[6] A. A. Solovev, S. Sanchez, M. Pumera, Y. F. Mei, and O. G. Schmidt, Adv. Funct. Mater. 20, 2430 (2010).

[7] K. E. Peyer, S. Tottori, F. Qiu, L. Zhang, and B. J. Nelson, Chem. Eur. J. 19, 28 (2012).

[8] V. V. Slastikov and C. Sonnenberg, IMA Journal of Applied Mathematics 77, 220235 (2012).

[9] D. D. Sheka, V. P. Kravchuk, and Y. Gaididei, Journal of Physics A: Mathematical and Theoretical 48, 125202 (2015).

[10] D. D. Sheka, I. A. Yastremsky, B. A. Ivanov, G. M. Wysin, and F. G. Mertens, Phys. Rev. B 69, 054429 (2004).

[11] D. D. Sheka, V. P. Kravchuk, K. V. Yershov, and Y. Gaididei, ArXiv e-prints (2015), 1502.06482